Porous Materials

DOI: 10.1002/anie.201310679

Mesoporous Prussian Blue Analogues: Template-Free Synthesis and Sodium-Ion Battery Applications**

Yanfeng Yue, Andrew J. Binder, Bingkun Guo, Zhiyong Zhang, Zhen-An Qiao, Chengcheng Tian, and Sheng Dai**

Abstract: *The synthesis of mesoporous Prussian blue analogues through a template-free methodology and the application of these mesoporous materials as high-performance cathode materials in sodium-ion batteries is presented. Crystalline mesostructures were produced through a synergistically coupled nanocrystal formation and aggregation mechanism. As cathodes for sodium-ion batteries, the Prussian blue analogues all show a reversible capacity of 65 mA h g^{-1} at low current rate and show excellent cycle stability. The reported method stands as an environmentally friendly and low-cost alternative to hard or soft templating for the fabrication of mesoporous materials.*

The rapidly growing use of intermittent energy sources such as solar and wind power to generate electricity necessitates the development of reliable, affordable, and efficient electric energy storage (EES) systems.[1,2] To date, advanced lithium-ion batteries have been considered to be the best choice for this application.[3,4] However, the high cost of lithium-ion batteries has restricted their application mainly to high-tech areas such as portable electronics and expensive electric vehicles. Furthermore, there is increasing concern that the world's lithium reserves may not be sufficient to meet the huge demands of the oncoming electric energy era. Sodium-ion batteries belong to a new generation of EES systems and work on the same principle as lithium-ion batteries. Compared with lithium, sodium is an abundant, low-cost element, thus making sodium-ion batteries more economical and more suitable for large-scale EES applications.[5] However, a drawback for the sodium-ion battery is the relatively large ionic radius of sodium (1.02 Å for sodium vs. 0.76 Å for lithium), which leads to insufficient mobility of the cations in a host with closely packed oxide ions.[6] Compared to traditional electrode materials, open-framework materials such as Prussian blue and its analogues have interstitial spaces larger than sodium ions, thus making them more suitable as electrodes for sodium-ion batteries.[7]

Prussian blue ($A[Fe^{III}Fe^{II}(CN)_6]$, $A = Na^+$ or K^+), one of the oldest synthetic coordination compounds, has a cubic face-centered structure (space group symmetry $Fm\bar{3}m$).[8] The open-framework structure consists of Fe^{II} and Fe^{III} ions sitting on alternate corners of corner-shared octahedra bridged by small conjugated cyanide anions ($C{\equiv}N^-$; Scheme 1a). In this structure, the low-spin ferrous ions bond to the carbon atoms and the high-spin ferric ions bond to the nitrogen atoms with bond lengths of 1.92 and 2.05 Å, respectively.[9] This forms a large ionic channel along the ⟨100⟩ direction; and since only half of the "A sites" in the $A[Fe^{III}Fe^{II}(CN)_6]$ structure are occupied, the structure allows the facile insertion and extraction of alkali-metal cations.[10] Upon the insertion/extraction of alkali-metal cations, there is a corresponding reduction/oxidation of some of the Fe^{III}/Fe^{II} ions, a reaction that creates the potential for using these materials as battery electrodes.[11] Prussian blue analogues contain transition-metal M^{II} ions in the place of the Fe^{II} centers, with compounds consisting of Fe^{III}–C≡N–M^{II} or Fe^{II}–C≡N–M^{II}.[7,12]

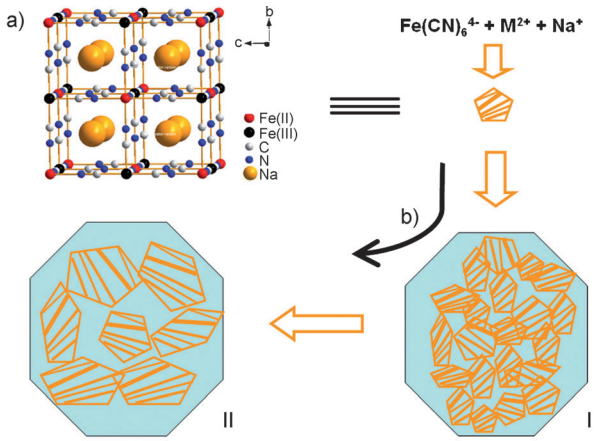

Scheme 1. The framework of Prussian blue (a) and a schematic illustration of the transformation from a mesoporous structure (I) to a macroporous structure (II) by a nanoparticle aggregation-based formation mechanism.

The electrochemical activities of Prussian blue and its analogues were investigated several years ago, first with Prussian blue films as hosts for alkali-metal ions[13] and then with nanocomposite $Na_4Fe(CN)_6/C$[14] or nanoparticulate $KNiFe(CN)_6$ (NiHCF)[15] morphologies. However, the thin electrodeposited Prussian blue films, with thicknesses of

[*] Dr. Y. Yue, Dr. B. Guo, Dr. Z. Zhang, Dr. Z.-A. Qiao, Prof.Dr. S. Dai
Chemical Sciences Division, Oak Ridge National Laboratory
Oak Ridge, TN 37831 (USA)
E-mail: guobkun@hotmail.com
dais@ornl.gov
A. J. Binder, C. Tian, Prof.Dr. S. Dai
Department of Chemistry, University of Tennessee
Knoxville, TN 37996 (USA)

[**] This research was supported by the U.S. Department of Energy's Office of Basic Energy Science, Division of Materials Sciences and Engineering, under contract with UT-Battelle, LLC.

Supporting information for this article is available on the WWW under http://dx.doi.org/10.1002/anie.201310679.

approximately 100 nm, were too thin for practical batteries. The $Na_4Fe(CN)_6$/C nanocomposite and crystalline NiHCF nanoparticles have been demonstrated to have an ultralong cycle life and a high rate capability, thus making these materials suitable for use as low-cost and pollution-free cathodes for sodium-ion batteries. Introducing extra mesoporosity into the framework of Prussian blue analogues will further enhance their performance by providing large channels for facile Na^+ mass transportation in the electrode, thereby reducing the sluggish solid-state diffusion.[16,17] Accordingly, there is a strong need for the development of synthesis methodologies for the generation of mesoporosity in Prussian blue and its analogues.

There have been several attempts to synthesize nanoporous Prussian blue analogues. Notably, Hu et al. have developed an interesting stepwise "crystal growth and etching" strategy for the synthesis of nanoporous Prussian blue analogues through exploitation of their low chemical stability in acidic media.[18] However, no uniform and stable mesoporous structures have been observed. Herein, we report the synthesis of mesoporous Prussian blue and its analogues through a template-free methodology and the application of these mesoporous materials as high-performance cathode materials in sodium batteries. The essence of our methodology lies in the formation of crystalline mesostructures through a synergistically coupled nanocrystal formation and aggregation mechanism. Hierarchically porous metal–organic frameworks (MOFs) with sponge-like structures have been fabricated through this formation mechanism without the use of a templating agent.[19] More importantly, both the surface morphology and the porosity of the MOFs can be tailored by etching the pore walls with the synthesis solvent using different reaction times. By using this bottom-up fabrication methodology, we successfully synthesized a series of hierarchical porous Prussian blue analogues by using different reaction times (NiHCF/*t*, where *t* stands for the reaction time in hours). The aggregation-based formation mechanism is presented in Scheme 1b. First, the reaction between the transition metal ions and $Fe(CN)_6^{4-}$ enables nanocrystals to form, aggregate, and join together.[20] Second, or possibly concurrently, the aggregates grow and eventually become single-grained particles. Finally, the stacked mesopores are transformed into macropores over longer reaction times.

The as-synthesized meso/macroporous NiHCF/*t* series prepared with different reaction times were crystalline and were found to have X-ray diffraction (XRD) spectra corresponding to a phase-pure face-centered cubic structure (Figure S1 in supporting information).[15] The broadening of the powder XRD peaks for the product resulting from a short reaction time (NiHCF/2) suggests that the Prussian blue crystals forming the pore walls were smaller or had a lower degree of periodicity than those resulting from longer reaction times. Furthermore, the calculated crystallite sizes of NiHCF/2 and NiHCF/18 were 11 and 13 nm, respectively. The biggest crystallites (26 nm) were observed for NiHCF/72, thus indicating a higher degree of periodicity and crystallinity with the longer reaction times. The mesoporous structures of the NiHCF/*t* series were demonstrated by scanning electron microscopy (SEM) and transmission electron microscopy (TEM; Figure 1). As observed in the SEM images (Figure 1a,c), continuous networks of NiHCF/2 and NiHCF/18 formed, with disordered mesopores that correspond to the aggregation of the nanosized particles (TEM images; Figure 1b,d). In the case of NiHCF/72, the mesopores finally enlarged to textural macropores, which were formed by packing of the single-grained nanosized particles (Figure 1e,f). The observations in the TEM images are consistent with the changes in the powder XRD peak intensities (Figure S1). The NiHCF/*t* series were characterized by Fourier transform infrared (FT-IR) spectroscopy, and the FT-IR spectra showed the characteristic C≡N stretch at 2090 cm^{-1} (Figure S2).[21] The molar Na/Fe/Ni ratios of the NiHCF/*t* series were obtained by inductively coupled plasma (ICP) analysis; and the molar ratios were calculated to be 1.41:0.91:1.00, 1.73:0.98:1.00 and 1.01:1.02:1.00 for NiHCF/2, NiHCF/18, and NiHCF/72, respectively.

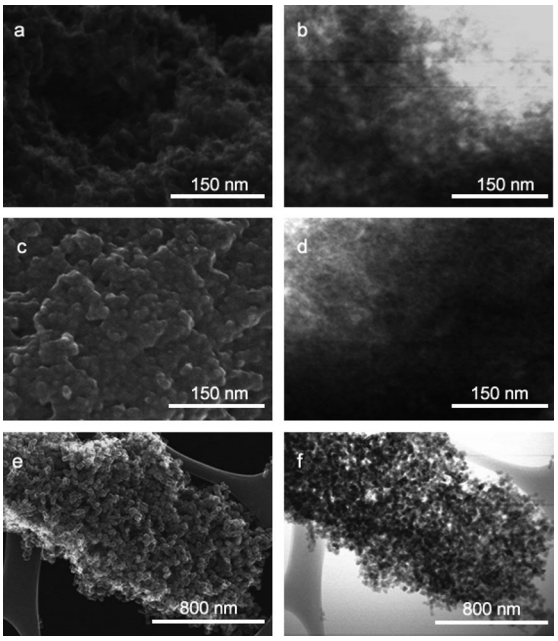

Figure 1. SEM (a, c, e) and TEM (b, d, f) images for the porous NiHCF series obtained after 2 h (top), 18 h (middle), and 72 h (bottom).

Three members of the NiHCF/*t* series obtained at different reaction times exhibited accessible porosity, as confirmed by nitrogen adsorption–desorption isotherms (Figure 2). Before the gas sorption measurements, lattice guest molecules were removed by solvent exchange, followed by thermal activation at 150 °C under flowing N_2. Type IV isotherms with hysteresis loops characteristic of large constricted mesopores were observed for the NiHCF/2 and NiHCF/18 samples, with widths in the range of 5 to 35 nm (Figure 2, inset). The Brunauer-Emmett-Teller (BET) surface areas were 299, 233, and 93 $m^2 g^{-1}$ for NiHCF/2, NiHCF/18, and NiHCF/72, respectively. Under exceptionally long reaction times (NiHCF/72), the mesopores were greatly enlarged and finally became macropores (> 45 nm), which were built up by packing of the relatively larger particles, as shown in the SEM images (Figure 1e).

Coin cells (2032) with sodium foil as a counter electrode were used to evaluate the electrochemical performance of the

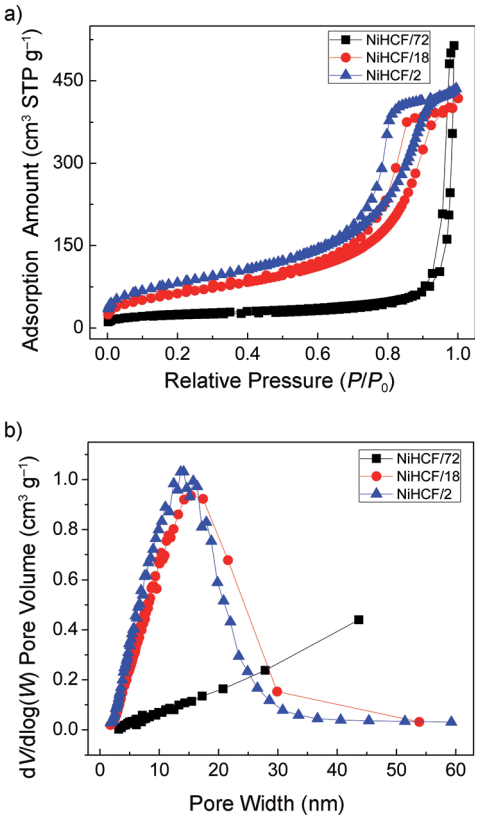

Figure 2. N_2 −196 °C isotherms of the NiHCF/*t* series (a) and corresponding BJH pore-size distribution (PSD) curves (b).

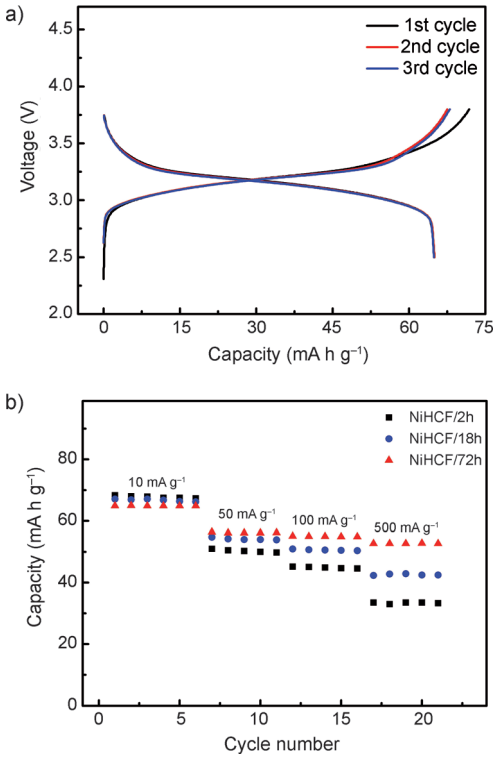

Figure 3. Charge/discharge curves for the NiHCF/72 sample (a) and rate performance for the NiHCF/*t* series (b).

as-synthesized materials. All cells were cycled between 2.5 and 3.8 V. Figure 3a and Figure S3 show the charge/discharge curves of this series of samples at a current rate of 10 mA g^{-1}. One charge plateau and one discharge plateau at around 3.2 V are observed in the charge/discharge curves and can be assigned to the Fe^{III}/Fe^{II} redox couple, as noted in previous reports.[7,22] These three samples displayed almost identical reversible capacities of around 65 mA h g^{-1} at the low current rate (Figure 3b). However, the capacity is lower than that reported for sodium manganese hexacyanoferrate,[7a] perhaps because the redox reaction of the Ni^{III}/Ni^{II} couple occurs with difficulty between 2.5 and 3.8 V. As a result of their porous structures, all of the samples displayed good rate performance. It is interesting that although NiHCF/72 has the smallest surface area, it displays the best rate performance. For instance, the specific discharge capacity of NiHCF/72 is as high as 55 mA h g^{-1} at 100 mA g^{-1} and 52 mA h g^{-1} at 500 mA g^{-1}. Clearly, the large pore diameter of NiHCF/72 is more efficient for sodium-ion transport. In addition, all three samples displayed excellent cycle stability at a high current rate of 100 mA g^{-1}, and no capacity loss was observed after 180 cycles (Figure S4). As reported, pore size plays an important role in the determination of the rate performance of nanoporous materials.[23] Large pores enable more facile Na^+ diffusion into the particle bulk through the filled electrolyte, thus improving the rate performance. We have observed this behavior in the NiHCF/*t* series; an increase in rate performance with increasing pore diameter consistent with the expectation that large pores permit more facile Na^+ transport in the electrolyte within the pores.

In summary, mesoporous Prussian blue analogues, NiHCF/*t*, were successfully synthesized by using a facile template-free solution method at room temperature, and a nanoparticle aggregation-based formation mechanism is suggested. The surface morphology, porosity, and crystallinity of the Prussian blue analogues can be modified by extending the reaction time. At different reaction stages, nanocrystal formation, aggregation, and grain growth occur; accordingly, the interconnected mesopores eventually transform into stacked macropores. As cathodes for sodium-ion batteries, all the NiHCF/*t* analogues show a reversible capacity of 65 mA h g^{-1} at low current rate and show excellent cycle stability. The macroporous NiHCF/72 with its smaller surface area displayed the best rate performance, maybe because it had the largest pores to facilitate more effective Na^+ mass transport.

These results have important implications for the fabrication of meso/macroporous electrode materials, in which the porous structure has a great effect on the electrochemical properties. Particularly for materials with lower chemical and physical stability, the reported method stands as an environmentally friendly and low-cost alternative to hard or soft templating for the fabrication of mesoporous materials.

Experimental Section

A typical procedure for the preparation of the NiHCF/*t* series materials: A solution of nickel(II) acetate tetrahydrate (0.249 g,

1 mmol) in water (17.5 mL) and dimethylformamide (DMF; 2.5 mL) was added to a solution of sodium hexacyanoferrate(II) decahydrate (0.484 g, 1 mmol) and NaCl (0.7 g) in water (17.5 mL) and DMF (2.5 mL) with stirring. The mixture was stirred for the desired time at room temperature and the resulting precipitate was separated by centrifugation and subsequently washed with water and methanol. The resulting product was dried under vacuum at 60 °C overnight before FT-IR spectroscopy, ICP analysis, powder XRD, SEM, TEM, nitrogen adsorption–desorption measurements, and battery characterization. The product was named NiHCF/*t*, in which *t* stands for the reaction time in hours.

Electrochemical experiments were carried out by using coin cells. The working electrode was prepared by mixing the as-synthesized materials, carbon black, and poly(vinylidenedifluoride) (PVDF) at a weight ratio of 70:20:10. The slurry was cast onto Al foil and dried under an infrared lamp to remove the solvent, followed by drying in a vacuum oven at 100 °C for 12 h. The loading of active materials was 1.5–2.0 mg cm^{-2}. Glass microfiber was used as a separator and sodium foil was used as both counter electrode and reference electrode. The electrolyte consisted of a solution of 1 M $NaClO_4$ in 1:1 (by volume) ethylene carbonate (EC)/propylene carbonate (PC). The cells were assembled in an argon-filled glove box with moisture and oxygen levels below 0.5 ppm. Galvanostatic discharge–charge experiments were conducted in the voltage range of 2.5–3.8 V on an Arbin battery test system.

Received: December 9, 2013
Published online: February 14, 2014

Keywords: aggregation · mesoporous materials · nanoparticles · Prussian blue · sodium-ion batteries

[1] a) M. Pasta, C. D. Wessells, R. A. Huggins, Y. Cui, *Nat. Commun.* **2012**, *3*, 1149; b) H. Pan, Y.-S. Hu, L. Chen, *Energy Environ. Sci.* **2013**, *6*, 2338 – 2360; c) H. Zhu, Z. Jia, Y. Chen, N. Weadock, J. Wan, O. Vaaland, X. Han, T. Li, L. Hu, *Nano Lett.* **2013**, *13*, 3093 – 3100.

[2] a) A. S. Aricò, P. Bruce, B. Scrosati, J.-M. Tarascon, W. V. Schalkwijk, *Nat. Mater.* **2005**, *4*, 366 – 377; b) Z. Yang, J. Zhang, M. C. W. Kintner-Meyer, X. Lu, D. Choi, J. P. Lemmon, J. Liu, *Chem. Rev.* **2011**, *111*, 3577 – 3613.

[3] a) J.-M. Tarascon, M. Armand, *Nature* **2001**, *414*, 359 – 367; b) W. Li, J. R. Dahn, D. S. Wainwright, *Science* **1994**, *264*, 1115 – 1118; c) J. B. Goodenough, K.-S. Park, *J. Am. Chem. Soc.* **2013**, *135*, 1167 – 1176; d) S. Yang, G. Cui, S. Pang, Q. Cao, U. Kolb, X. Feng, J. Maier, K. Müllen, *ChemSusChem* **2010**, *3*, 236 – 239.

[4] a) J. B. Goodenough, Y. Kim, *Chem. Mater.* **2010**, *22*, 587 – 603; b) S. Lee, Y. Cho, H.-K. Song, K. T. Lee, J. Cho, *Angew. Chem.* **2012**, *124*, 8878 – 8882; *Angew. Chem. Int. Ed.* **2012**, *51*, 8748 – 8752; c) M. Armand, J.-M. Tarascon, *Nature* **2008**, *451*, 652 – 657; d) F. Han, D. Li, W.-C. Li, C. Lei, Q. Sun, A.-H. Lu, *Adv. Funct. Mater.* **2013**, *23*, 1692 – 1700.

[5] a) Y. Wang, X. Yu, S. Xu, J. Bai, R. Xiao, Y.-S. Hu, H. Li, X.-Q. Yang, L. Chen, X. Huang, *Nat. Commun.* **2013**, *4*, 3365; b) Y. Sun, L. Zhao, H. Pan, X. Lu, L. Gu, Y.-S. Hu, H. Li, M. Armand, Y. Ikuhara, L. Chen, X. Huang, *Nat. Commun.* **2013**, *4*, 2878; c) Z. Jian, L. Zhao, H. Pan, Y.-S. Hu, H. Li, W. Chen, L. Chen, *Electrochem. Commun.* **2012**, *14*, 86 – 89; d) L. Zhao, J. Zhao, Y.-S. Hu, H. Li, Z. Zhou, M. Armand, L. Chen, *Adv. Energy Mater.* **2012**, *2*, 962 – 965.

[6] a) C. Li, C. Yin, L. Gu, R. E. Dinnebier, X. Mu, P. A. van Aken, J. Maier, *J. Am. Chem. Soc.* **2013**, *135*, 11425 – 11428; b) R. D. Shannon, *Acta Crystallogr. Sect. A* **1976**, *32*, 751 – 767.

[7] a) L. Wang, Y. Lu, J. Liu, M. Xu, J. Cheng, D. Zhang, J. B. Goodenough, *Angew. Chem.* **2013**, *125*, 2018 – 2021; *Angew. Chem. Int. Ed.* **2013**, *52*, 1964 – 1967; b) X. Wu, Y. Cao, X. Ai, J. Qian, H. Yang, *Electrochem. Commun.* **2013**, *15*, 145 – 148; c) Y. Lu, L. Wang, J. Cheng, J. B. Goodenough, *Chem. Commun.* **2012**, *48*, 6544 – 6546; d) N. Imanishi, T. Morikawa, J. Kondo, R. Yamane, Y. Takeda, O. Yamamoto, H. Sakaebe, M. Tabuchi, *J. Power Sources* **1999**, *81 – 82*, 530 – 534.

[8] a) H. J. Buser, A. Ludi, W. Petter, D. Schwarzenbach, *J. Chem. Soc. Chem. Commun.* **1972**, 1299 – 1299; b) K. Tayan, I. Hida, *Acc. Chem. Res.* **1986**, *19*, 162 – 168; c) S. Margadonna, K. Prassides, A. N. Fitch, *Angew. Chem.* **2004**, *116*, 6476 – 6479; *Angew. Chem. Int. Ed.* **2004**, *43*, 6316 – 6319.

[9] a) M. Okubo, I. Honma, *Dalton Trans.* **2013**, *42*, 15881 – 15884; b) A. Ludi, H.-U. Güdel, M. Rüegg, *Inorg. Chem.* **1970**, *9*, 2224 – 2227.

[10] a) T. Matsuda, J. Kim, Y. Moritomo, *J. Am. Chem. Soc.* **2010**, *132*, 12206 – 12207; b) H. J. Buser, D. Schwarzenbach, W. Petter, A. Ludi, *Inorg. Chem.* **1977**, *16*, 2704 – 2710.

[11] a) D. Yang, X.-Z. Liao, B. Huang, J. Shen, Y.-S. He, Z.-F. Ma, *J. Mater. Chem. A* **2013**, *1*, 13417 – 13421; b) C. D. Wessells, S. V. Peddada, M. T. McDowell, R. A. Huggins, Y. Cui, *J. Electrochem. Soc.* **2012**, *159*, A98 – A103.

[12] a) D. Asakura, C. H. Li, Y. Mizuno, M. Okubo, H. Zhou, D. R. Talham, *J. Am. Chem. Soc.* **2013**, *135*, 2793 – 2799; b) C. D. Wessells, R. A. Huggins, Y. Cui, *Nat. Commun.* **2011**, *2*, 1563; c) M. Okubo, D. Asakura, Y. Mizuno, T. Kudo, H. Zhou, A. Okazawa, N. Kojima, K. Ikedo, T. Mizokawa, I. Honma, *Angew. Chem.* **2011**, *123*, 6393 – 6397; *Angew. Chem. Int. Ed.* **2011**, *50*, 6269 – 6273.

[13] V. D. Neff, *J. Electrochem. Soc.* **1978**, *125*, 886 – 887.

[14] J. Qian, M. Zhou, Y. Cao, X. Ai, H. Yang, *Adv. Energy Mater.* **2012**, *2*, 410 – 414.

[15] C. D. Wessells, S. V. Peddada, R. A. Huggins, Y. Cui, *Nano Lett.* **2011**, *11*, 5421 – 5425.

[16] a) E. M. Sorensen, S. J. Barry, H.-K. Jung, J. R. Rondinelli, J. T. Vaughey, K. R. Poeppelmeier, *Chem. Mater.* **2006**, *18*, 482 – 489; b) H. Liu, G. Wang, J. Liu, S. Qiao, H. Ahn, *J. Mater. Chem.* **2011**, *21*, 3046 – 3052.

[17] a) G. Wang, H. Liu, J. Liu, S. Qiao, G. M. Lu, P. Munroe, H. Ahn, *Adv. Mater.* **2010**, *22*, 4944 – 4948; b) P. G. Bruce, B. Scrosati, J.-M. Tarascon, *Angew. Chem.* **2008**, *120*, 2972 – 2989; *Angew. Chem. Int. Ed.* **2008**, *47*, 2930 – 2946.

[18] a) M. Hu, S. Furukawa, R. Ohtani, H. Sukegawa, Y. Nemoto, J. Reboul, S. Kitagawa, Y. Yamauchi, *Angew. Chem.* **2012**, *124*, 1008 – 1012; *Angew. Chem. Int. Ed.* **2012**, *51*, 984 – 988; b) M. Hu, N. L. Torad, Y. Yamauchi, *Eur. J. Inorg. Chem.* **2012**, 4795 – 4799; c) M. Hu, A. A. Belik, M. Imura, Y. Yamauchi, *J. Am. Chem. Soc.* **2013**, *135*, 384 – 391.

[19] Y. Yue, Z.-A. Qiao, P. F. Fulvio, A. J. Binder, C. Tian, J. Chen, K. M. Nelson, X. Zhu, S. Dai, *J. Am. Chem. Soc.* **2013**, *135*, 9572 – 9575.

[20] a) M. Y. Lin, H. M. Lindsay, D. A. Weitz, R. C. Ball, R. Klein, P. Meakin, *Nature* **1989**, *339*, 360 – 362; b) B. Ingham, T. H. Lim, C. J. Dotzler, A. Henning, M. F. Toney, R. D. Tilley, *Chem. Mater.* **2011**, *23*, 3312 – 3317.

[21] P. J. Kulesza, M. A. Malik, A. Denca, J. Strojek, *Anal. Chem.* **1996**, *68*, 2442 – 2446.

[22] a) Y. Mizuno, M. Okubo, E. Hosono, T. Kudo, K. Oh-ishi, A. Okazawa, N. Kojima, R. Kurono, S. Nishimurac, A. Yamadac, *J. Mater. Chem. A* **2013**, *1*, 13055 – 13059; b) Y. You, X.-L. Wu, Y.-X. Yin, Y.-G. Guo, *J. Mater. Chem. A* **2013**, *1*, 14061 – 14065.

[23] a) Y. Ren, A. R. Armstrong, F. Jiao, P. G. Bruce, *J. Am. Chem. Soc.* **2010**, *132*, 996 – 1004; b) M. D. Levi, D. Aurbach, *J. Phys. Chem. B* **1997**, *101*, 4641 – 4647.

